5300 *Chem. Mater.* **2009,** *21,* 5300–5306
DOI:10.1021/cm9024167

CHEMISTRY OF MATERIALS
Article

Hierarchically Porous Monolithic $LiFePO_4$/Carbon Composite Electrode Materials for High Power Lithium Ion Batteries

Cara M. Doherty,[†,‡] Rachel A. Caruso,*[,‡,§] Bernd M. Smarsly,[∥] Philipp Adelhelm,[⊥] and Calum J. Drummond*[,†,§]

[†]*CSIRO Molecular and Health Technologies, Private Bag 10, Clayton, Victoria 3169, Australia,* [‡]*The University of Melbourne, School of Chemistry, Victoria 3010, Australia,* [§]*CSIRO Materials Science and Engineering, Private Bag 33, Clayton, Victoria 3169, Australia,* [∥]*University of Giessen, Institute of Physical Chemistry, Heinrich-Buff-Ring 58, D-35392 Giessen, Germany, and* [⊥]*Utrecht University, Sorbonnelaan 16, 3584CA Utrecht, The Netherlands*

Received August 5, 2009. Revised Manuscript Received September 17, 2009

A novel method for the preparation of hierarchically porous $LiFePO_4$ electrode materials for lithium ion batteries has been investigated. A meso/macroporous carbon monolith, a conductive framework, was prepared and infiltrated with the $LiFePO_4$ precursors to increase the electrode/electrolyte interface and improve the rate capability of the battery. The final $LiFePO_4$/carbon monoliths feature a meso/macroporous hierarchical structure. The monoliths were calcined at increasing temperatures, from 650 to 800 °C, to determine the structural and sintering effects on the electrochemical properties of the materials. The samples were characterized using SEM, TEM, nitrogen sorption, and XRD analysis prior to electrochemical testing. The results showed that the capacity of the $LiFePO_4$/carbon electrodes achieved 82% of the theoretical capacity at 0.1C discharge rate.

Introduction

Lithium-ion batteries have become increasingly popular over the last two decades due to demand for portable energy storage devices. Lithium iron phosphate, $LiFePO_4$, is a promising cathode material due to its high theoretical capacity (170 mA h g^{-1}), relatively low cost for synthesis, and low environmental impact.[1,2] Further improvements in the properties of existing electrode materials will require design at the nano- to micrometer level.[3] Increasing the amount of electrode/electrolyte interface to enhance charge transport has the potential to improve the electrochemical properties of the lithium ion batteries. The use of porous electrode materials offers an efficient method for increasing the interfacial area and decreasing the lithium ion diffusion distance, allowing for fast charge transport and improved power capability.[4,5] Efficient access of the electrolyte into the electrode pores is essential to harness the advantages that porous electrode materials might offer.

Micropores, with diameters less than 2 nm, in materials can produce very high surface areas. However, they are easily blocked, may not allow efficient access of the electrolyte throughout the electrode, and therefore may not be ideal for electrode materials.[3] Electrode materials with slightly larger pores, mesopores in the range 2−50 nm, also offer high surface areas while potentially avoiding the permanent trapping of lithium ions that is possible with micropores.[6] Producing hierarchically porous electrodes which feature both macropores (> 50 nm) and mesopores has the potential to provide easy access of electrolyte ions to the electrode structure. The continuous macroporous network allows an efficient transport route for the solvated ions to get to the mesopores and hence may offer superior battery performance.[6]

Nanocasting of hard templates has proved to be an effective way to prepare monolithic materials which can provide high surface areas and an open porous structure.[6−9] Hierarchical silica and carbon monoliths have been developed since the early 1990s using sol−gel synthesis to prepare the hard silica template and then a nanocasting technique to produce the carbon monolith.[7−12] Forming a porous $LiFePO_4$ monolith

*Corresponding authors. C.J.D.: e-mail calum.drummond@csiro.au, tel. +61 3 9545 2057, fax +61 3 9545 2059. R.A.C.: e-mail: rcaruso@unimelb.edu.au, tel. +61 3 8344 7146, fax +61 3 9347 5180.

(1) Padhi, A. K.; Nanjundaswamy, K. S.; Masquelier, C.; Okada, S.; Goodenough, J. B. *J. Electrochem. Soc.* **1997**, *144*, 1609–1613.
(2) Padhi, A. K.; Nanjundaswamy, K. S.; Goodenough, J. B. *J. Electrochem. Soc.* **1997**, *144*, 1188–1194.
(3) Wang, Z. Y.; Li, F.; Ergang, N. S.; Stein, A. *Chem. Mater.* **2006**, *18*, 5543–5553.
(4) Long, J. W.; Dunn, B.; Rolison, D. R.; White, H. S. *Chem. Rev.* **2004**, *104*, 4463–4492.
(5) Attard, G. S.; Elliott, J. M.; Bartlett, P. N.; Whitehead, A.; Owen, J. R. *Macromol. Symp.* **2000**, *156*, 179–186.
(6) Hu, Y. S.; Adelhelm, P.; Smarsly, B. M.; Hore, S.; Antonietti, M.; Maier, J. *Adv. Funct. Mater.* **2007**, *17*, 1873–1878.
(7) Nakanishi, K.; Soga, N. *J. Am. Ceram. Soc.* **1991**, *74*, 2518–2530.
(8) Nakanishi, K.; Soga, N. *J. Non-Cryst. Solids* **1992**, *139*, 1–13.
(9) Taguchi, A.; Smatt, J. H.; Linden, M. *Adv. Mater.* **2003**, *15*, 1209–1211.
(10) Minakuchi, H.; Nakanishi, K.; Soga, N.; Ishizuka, N.; Tanaka, N. *Anal. Chem.* **1996**, *68*, 3498–3501.
(11) Yang, H. F.; Shi, Q. H.; Liu, X. Y.; Xie, S. H.; Jiang, D. C.; Zhang, F. Q.; Yu, C. Z.; Tu, B.; Zhao, D. Y. *Chem. Commun.* **2002**, *23*, 2842–2843.
(12) Yu, C. Z.; Fan, J.; Tian, B. Z.; Zhao, D. Y.; Stucky, G. D. *Adv. Mater.* **2002**, *14*, 1742–1745.

 Published on Web 10/12/2009

directly using surfactant self-assembly and sol−gel techniques is difficult as the templating technique requires a phase separation of the inorganic precursor in the presence of the water-soluble polymers. Once the materials have condensed into two phases, they are calcined to remove the templating polymers and crystallize the inorganic framework. The crystallization process for $LiFePO_4$ causes the mesopore structure to collapse due to crystal growth and reduced support from the decomposition of the soft polymer template. Silica has the advantage that it remains amorphous when fired at 600 °C and is able to withstand the high calcination temperatures and maintain a porous monolithic structure. Carbon requires a rigid template to be able to maintain a porous monolithic structure during the carbonization process at temperatures above 700 °C.[13] Silica offers a robust structure that remains intact during the carbonization process which can then be removed chemically leaving behind a porous carbon monolith.

Employing sol−gel and nanocasting templating techniques to prepare lithium iron phosphate monolithic electrode materials has proved to be challenging. $LiFePO_4$ could not be templated directly with a silica monolith as it dissolved when washed with HF during the silica template removal and chemically reacted when washed with NaOH. Also $LiFePO_4$ could not be templated with a carbon monolith as removal of the carbon template in the presence of oxygen caused the $LiFePO_4$ to oxidize into $Li_3Fe_2PO_4$ and other impurity phases.

An alternative approach involves the synthesis of a $LiFePO_4$/carbon composite as an electrode material in which the hierarchically porous carbon monolith provides a robust, conductive framework into which the lithium iron phosphate can infiltrate (Scheme 1). Maintaining a macro/mesoporous composite can potentially offer enhanced electrolyte access to the high interfacial areas which may improve the charge transport and power capability. This method of preparing electrodes offers a novel methodology of incorporating nanostructures into electrode materials. Instead of the traditional method of adhering nanoparticles/nanostructures to a flat current collector, the current collector becomes the nanostructured material onto which the electrode material is coated. This method could potentially remove the need for the addition of conductive and binding agents during the preparation of the electrodes which offers a significant advantage. Here we describe the development of electrode monoliths which feature a hierarchical macro/mesoporous continuous open network. This study is a part of a body of work dedicated to building a better understanding of the link between nanostructured porous $LiFePO_4$ electrode materials and the electrochemical performance in Li-ion batteries.[14,15]

Experimental Section

Preparation of Silica and Carbon Monoliths. The silica monoliths that featured the hierarchical porous network were prepared using the Nakanishi process as described in the literature.[6,7,16] The carbon monoliths were prepared via a nanocasting technique in which the preformed silica monolith was infiltrated with a carbon precursor, the carbon/silica monolith was carbonized at 700 °C under N_2, and then the silica was removed leaving behind a porous carbon monolith. The synthesis procedure follows that developed by Hu et al.[6] Mesophase pitch (MP) from Mitsubishi Chemical Gas Company was used as the carbon precursor as it carbonizes very well and features low micropore content compared to other carbon sources such as furfuryl alcohol and sucrose solution. Hu et al. were able to synthesize hierarchical meso- and macroporous carbon monoliths from the mesophase pitch which featured both high surface areas and well developed graphitic carbon microstructures.[6] The carbon monoliths showed remarkable electrochemical performance as an anode in lithium ion batteries and therefore offer a promising conductive nanostructure for the $LiFePO_4$/carbon composite material.

Scheme 1. Schematic of Nanocasting Technique Used To Prepare a $LiFePO_4$/Carbon Composite Monolith[a]

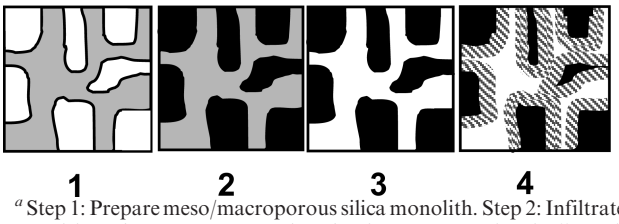

[a] Step 1: Prepare meso/macroporous silica monolith. Step 2: Infiltrate pores with carbon precursor and carbonize. Step 3: Chemically etch away silica monolith. Step 4: Infiltrate $LiFePO_4$ precursor into pores and calcine.

Synthesis of $LiFePO_4$/Carbon Composites. The $LiFePO_4$/carbon composite was synthesized by infiltrating the lithium iron phosphate precursor solution into the preformed hierarchically porous carbon monolith. The $LiFePO_4$ solution was prepared using water based solution chemistry, and the precursors were chosen so that the solution would not precipitate prior to infiltration. Stoichiometric amounts (5 mmol) of iron nitrate nonahydrate ($Fe(NO_3)_3 \cdot 9H_2O$, Aldrich) were dissolved into 10 mL of deionized water, and then the lithium acetate ($LiC_2H_3O_2$, Aldrich) and phosphoric acid (H_3PO_4, Sigma-Aldrich) were added; the solution was stirred for 2 h to ensure homogeneity. Several samples were prepared with two types of nonionic triblock copolymers. F108 ($(EO)_{132}(PO)_{60}(EO)_{132}$, Fluka) and F127 ($(EO)_{106}(PO)_{70}(EO)_{106}$, Sigma-Aldrich) were added in 0.01 and 0.02 mol quantities to the lithium iron phosphate precursor solution respectively and stirred for 2 h.

A total of 0.2 g of carbon monolith was placed in an open glass boat together with the water based lithium iron phosphate precursor solution. Approximately 0.025 mol of the precursor lithium iron phosphate solution was infiltrated per 1 g of carbon monolith. Excess lithium iron phosphate precursor solution was used to ensure maximum loading into the carbon monolith, which gave approximately 50% final loading by weight. The boat was gently horizontally agitated at room temperature allowing slow evaporation of the precursor solution while infiltrating the porous carbon monolith. Once the precursor solution had evaporated down to a viscous gel, the loaded monolith was removed and the excess solution scraped from the outside. The monolith was further dried at 40 °C and then heated at 1 °C per min to the required calcination temperature and held there for 6 h. The samples were sintered under a

(13) Lee, J.; Kim, J.; Hyeon, T. *Adv. Mater.* **2006**, *18*, 2073–2094.
(14) Doherty, C. M.; Caruso, R. A.; Smarsly, B. M.; Drummond, C. J. *Chem. Mater.* **2009**, *21*, 2895–2903.
(15) Doherty, C. M. PhD Thesis, The University of Melbourne, **2009**
(16) Sonnenburg, K.; Adelhelm, P.; Antonietti, M.; Smarsly, B.; Noske, R.; Strauch, P. *Phys. Chem. Chem. Phys.* **2006**, *8*, 3561–3566.

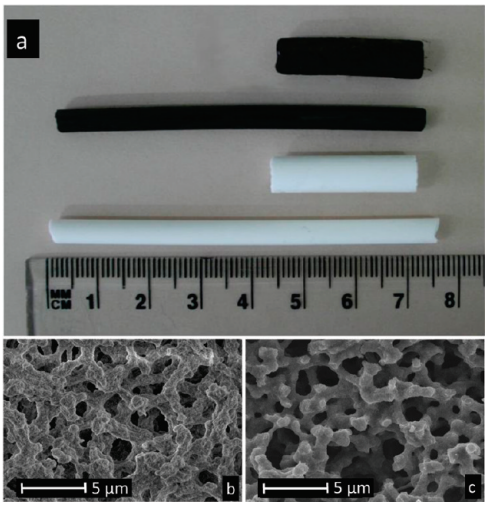

Figure 1. (a) Photograph showing two different diameter silica monoliths (white) prepared via the Nakanishi process and the subsequent carbon monoliths (black) nanocast from the silica monoliths. (b) SEM image of the silica monolith and (c) SEM image of the carbon monolith.

reducing atmosphere (5% hydrogen in argon) to avoid the formation of Fe^{3+} impurities. Various calcination temperatures were trialed (650, 700, 750, and 800 °C) to determine the optimal temperature for the monolithic samples.

Characterization. Powder X-ray diffraction (XRD) was performed with the Philips X'Pert Pro diffractometer using Co Kα radiation. The surface areas and pore distributions of samples were determined via nitrogen sorption with the Micromeritics Tristar surface area and porosity analyzer. The samples were degassed under vacuum (≤100 mTorr) at 150 °C for 16 h prior to analysis. The surface area was calculated using the Brunauer−Emmet−Teller (BET) method, and the Barrett−Joyner−Halenda (BJH) pore size distribution was determined using the desorption branch of the isotherm. Field emission scanning electron microscopy (SEM) was performed at 5 kV, and transmission electron microscopy (TEM) was undertaken at the Australian Nuclear Science and Technology Organisation (ANSTO) using a JEOL 2012F. The carbon content was determined using a Carlo Erba Elemental Analyzer EA 1108 from The Campbell Microanalytical Laboratory, Department of Chemistry, University of Otago, Dunedin, New Zealand.

Electrochemical Analysis. The $LiFePO_4$ electrode slurries comprised 75% active material, 15% Shawinigan carbon black, 10% Kuruha Polyvinylidene Fluoride (PVDF) binder, and *N*-methyl-2-pyrrolidinon anhydrous (NMP, Sigma-Aldrich) solvent. The electrode slurry was coated onto the aluminum current collector using a k-bar and achieved loading of ∼1 mg cm^{-2}. The electrode was then dried overnight under vacuum at 120 °C. The electrodes were tested in a CR2032 coin cell with 1 M $LiPF_6$ electrolyte (Hohsen) in 1:1 (v/v) ethylene carbonate/diethyl carbonate (EC:DEC), a Teflon Celgard separator (#2400, 16 mm diameter), and lithium ribbon (Sigma-Aldrich).

Electrochemical testing was undertaken using a Solartron 1470E multichannel Cell Test potentiostat. To keep the results consistent, the currents were calculated on the active material only; hence, the mass of the carbon was subtracted. Impedance measurements were carried out after the coin cells had been galvanostatically cycled 18 times to ensure that the solid electrolyte interface layer on the cathode had been fully developed and stabilized. An amplitude AC signal of 5 mV and frequency in the range 100 kHz−0.01 Hz was used on the cells in the full state of discharge.

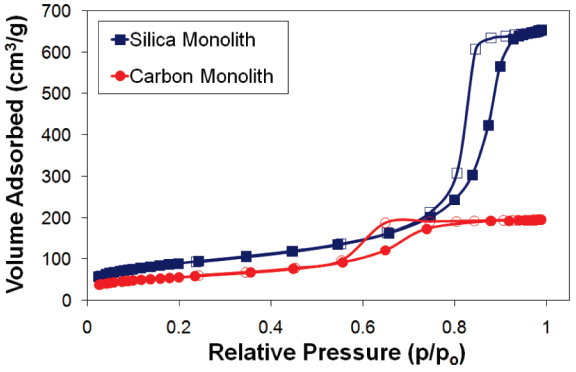

Figure 2. (a) Nitrogen sorption isotherms for the silica and carbon monolith templates.

Results and Discussion

The silica template and the resulting carbon monoliths are pictured in Figure 1a. These silica monoliths were obtained by the process introduced by Nakanishi and Soga.[7,8] As the photograph shows, a range of diameters and lengths can be achieved for the silica and, hence, the carbon monoliths.

The SEM image in Figure 1b shows the coral-like macroporous structures of the silica monoliths prepared using the sol−gel Nakanishi process. The interconnected macroporous network was formed during hydrolysis and condensation of the tetramethylorthosilicate solution due to the phase separation of the inorganic precursor in the presence of the water-soluble polymers. The micrometer sized branches contained mesopores with diameters of 10−12 nm. The mesopores were formed after gelation and developed during the aging, solvent exchange, and drying processes.[17] The associated carbon monoliths nanocast from the silica templates are pictured in Figure 1c. They also featured micrometer sized branches with good interconnectivity which is ideal for electrolyte access into the mesopores contained in the structure. The micrometer sized branches created a continually interconnected macroporous structure and featured mesopores with 5 nm diameter.

The nitrogen sorption results in Figure 2 shows the different isotherms for the silica monolith and the associated nanocast carbon monolith. The BET surface area of the silica monoliths was 320 $m^2\ g^{-1}$ with a mesopore volume of 1.0 $cm^3\ g^{-1}$. The BET surface area was 200 $m^2\ g^{-1}$ for the resulting carbon monolith, and the mesopore volume decreased to a third of that of the silica templates to 0.3 $cm^3\ g^{-1}$. The average mesopore diameter also was reduced from 11 to 5 nm due to the nanocasting technique (see the Supporting Information, Figure S1).

The advantage of using a carbon monolith prepared from mesophase pitch is that the resulting material has a relatively higher graphite-like ordered carbon structure which provides improved conductivity and does not feature the micropores present when forming carbon structures with alternative carbon source such as sucrose

(17) Nakanishi, K.; Shikata, H.; Ishizuka, N.; Koheiya, N.; Soga, N. *J. High Resolut. Chromatogr.* **2000**, *23*, 106–110.

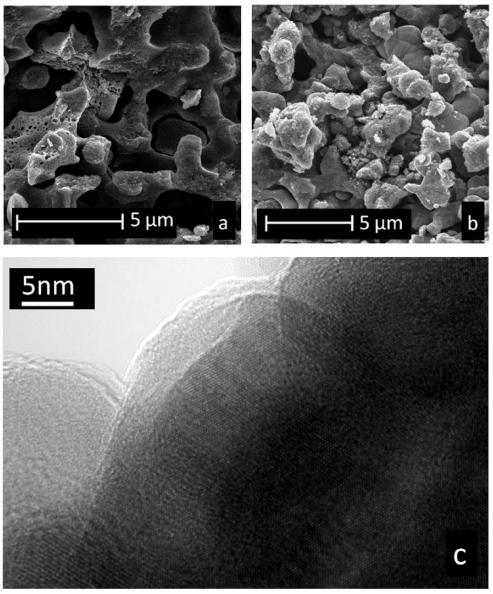

Figure 3. SEM images of $LiFePO_4$/carbon monoliths calcined at (a) 650 °C and (b) 750 °C. (c) TEM image of monolith composite calcined at 650 °C.

or fructose.[6] Also, mesophase pitch as carbon precursor possess a lower content of other elements such as oxygen and hydrogen, for example, compared to sugars serving as carbon precursor. The carbon monolith provides a highly conductive framework with the optimal porosity for electrochemistry into which the $LiFePO_4$ can infiltrate.[6]

Characterization of $LiFePO_4$/Carbon Composites. The position of the $LiFePO_4$ within the composite structure will impact significantly on the electrochemical results, as efficient penetration into the macro/mesopores will provide increased interfacial surfaces and more intimate contact with the carbon monolith which essentially acts as the current collector.

All monolith composite samples were able to withstand the calcination process without breaking or cracking. The samples were ground to complete the XRD analysis and prepared into electrode films for electrochemical analysis. Figure 3a,b shows the SEM images for the $LiFePO_4$/carbon composite samples which were calcined respectively at 650 and 750 °C. The $LiFePO_4$ intertwines through the branched carbon structure, mostly filling in the large macropores making the structure much denser than the carbon template seen in Figure 1c. The TEM results of the $LiFePO_4$/carbon composite show the presence of crystalline lattice positioned between amorphous carbon (Figure 3c).

Figure 4 shows the XRD results for the samples calcined at increasing temperatures. The broad maximum between 25° and 35° 2θ was due to the presence of nongraphitic carbon in the samples which was determined to be approximately 50 wt % via elemental analysis. The narrowing of the peaks occurs as the calcination temperature was increased due to the increase in $LiFePO_4$ crystallite diameter from 51 to 105 nm (Table 1).

The nitrogen sorption analysis revealed information about the infiltration of the $LiFePO_4$ into the carbon mesopores. Table 1 contains the BET surface areas and

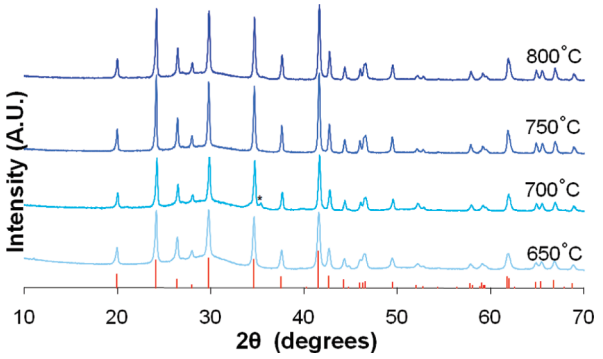

Figure 4. XRD analysis for the $LiFePO_4$/carbon composite samples which were calcined at various temperatures. The peaks are indexed to $LiFePO_4$, and a trace amount of iron phosphate is indicated by the asterisk.

pore volumes for each of the samples. The BET surface areas and pore volumes dropped from 200 $m^2\ g^{-1}$ and 0.3 $cm^3\ g^{-1}$ with the carbon monolith by up to 30% for the $LiFePO_4$/carbon samples due to the filling of pores after $LiFePO_4$ infiltration.

Figure 5a shows the isotherms for the carbon and $LiFePO_4$/carbon monoliths calcined at 700 °C. The reduced uptake proves that a certain fraction of the porosity is filled or blocked by $LiFePO_4$, resulting in a reduced surface area and reduced mesopore volume. The isotherm for the carbon monolith shows no uptake of nitrogen at relative pressures above 0.8, because the macropores are quite large and thus not detected by a standard nitrogen sorption experiment. In comparison, for the $LiFePO_4$/carbon monolith (Figure 5a), there is an increase in the volume of nitrogen adsorbed at $p/p_0 > 0.8$, indicating that the macropores were partially filled, as smaller voids remained in this material which can now be detected with N_2 sorption.

The change in the sample porosity in the $LiFePO_4$/carbon monolith is likely due to either filling or blockage of the pores of the initial carbon monolithic structure due to $LiFePO_4$ infiltration. The decrease in pore volume is not due to pore collapse within the carbon monolith as the monolithic pore structure is not affected at these temperatures. The $LiFePO_4$/carbon monoliths had very similar isotherms when calcined at temperatures between 650 and 800 °C (see the Supporting Information, Figure S2). Each of the samples calcined at increasing temperatures had similar isotherms indicating that crystallite growth was not significantly changing the porosity of the composite material.

The desorption pore size distribution in Figure 5b shows a gradual decrease in pore volume at the 5 nm diameter peaks as the calcination temperatures were increased, which was likely due to pore blockage or complete filling. Figure 5b specifically indicates that the 5 nm pore volumes were reduced; however, the pore size did not decrease as there was no evidence that smaller pores ranging below 5 nm were present, as would be expected if the $LiFePO_4$ was able to substantially fill the carbon mesopores.

Electrochemical Analysis of $LiFePO_4$/Carbon Composites. Each of the samples was prepared into electrodes and cycled three times at different c-rates of 0.1C, 0.2C,

Table 1. Pore Volumes and BET Surface Areas Determined by Nitrogen Sorption and Crystallite Sizes As Determined with XRD Rietveld Analysis for the $LiFePO_4$/Carbon Composite Samples

calcination temperature [°C]	BET surface area [$m^2\ g^{-1}$]	BJH pore volume [$cm^3\ g^{-1}$]	crystallite diameter [nm]
650	140	0.22	51
700	160	0.27	77
750	150	0.26	94
800	140	0.26	105

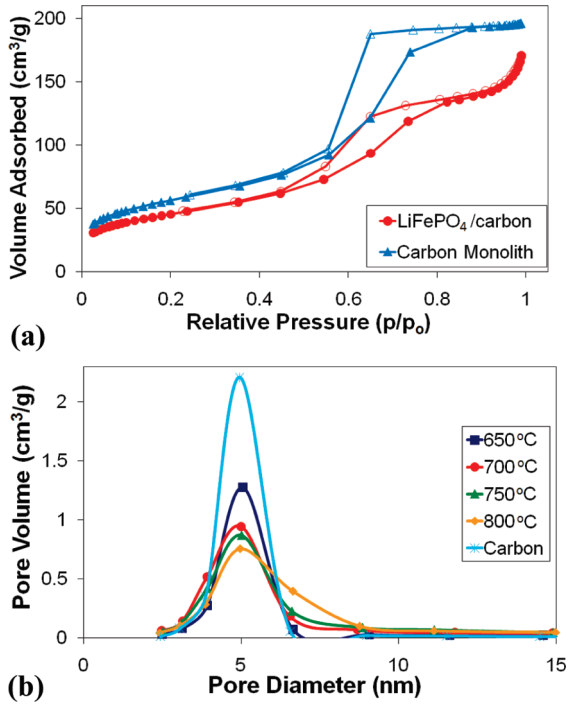

Figure 5. (a) Nitrogen sorption isotherms for $LiFePO_4$/carbon monolith composite calcined at 700 °C compared with that of the carbon monolith (also calcined at 700 °C). The filled markers denote the adsorption branch and the empty markers denote the desorption branch. (b) BJH desorption pore size distribution for the $LiFePO_4$/carbon monolith samples calcined at increasing temperatures including the carbon monolith for comparison. The results refer to the nitrogen uptake per gram of sample ($LiFePO_4$/carbon).

1C, 2C, and 5C. The c-rates were calculated from the mass of $LiFePO_4$ with the amount of carbon being subtracted. The discharge capacities for the $LiFePO_4$/carbon composites are presented in Figure 6a. The calcination temperature had a significant effect on the capacity of the coin cells. The optimal temperature was determined to be 750 °C with capacity of 140 mA h g^{-1} attained at a discharge rate of 0.1C and 100 mA h g^{-1} at 5C which compares to the theoretical capacity for $LiFePO_4$ of 170 mA h g^{-1}. This difference is likely due to the structural features of the composite material. The discharge profiles in Figure 6b have noticeably curved profiles even at the slow discharge rate of 0.1 C. The 3.4 V voltage plateau drops as the cell discharges due to polarization. This is due to the diffusion resistance within the composite electrode.[18,19] Although there was an abundance of conductive carbon provided by the carbon

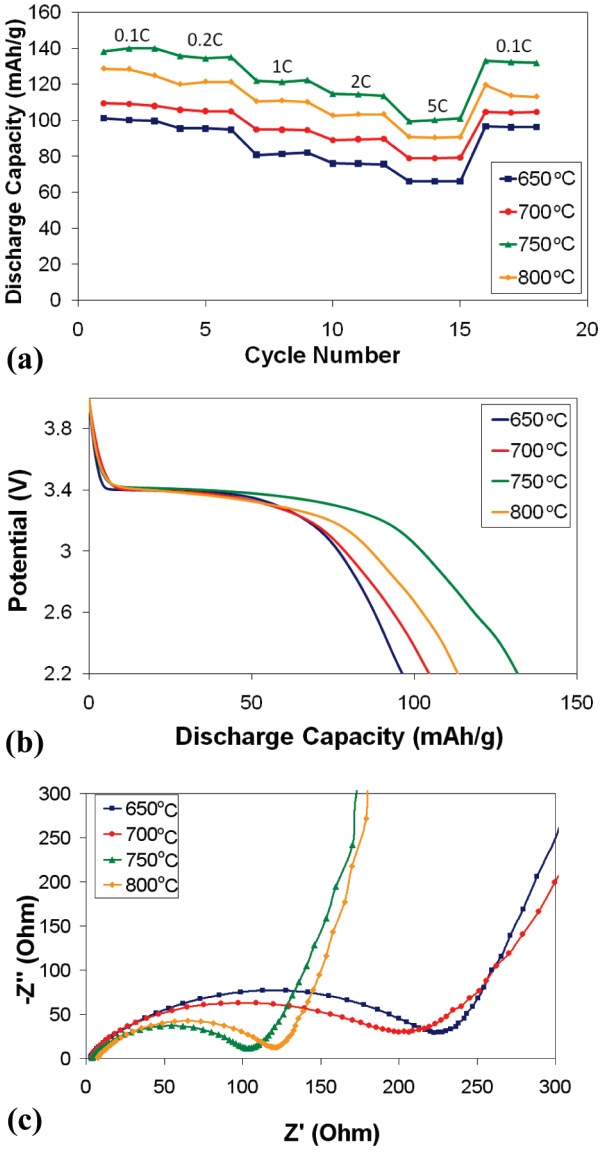

Figure 6. (a) Discharge capacity, (b) discharge profile at 0.1C discharge rate, and (c) AC impedance spectroscopy for $LiFePO_4$/carbon monolith samples that were calcined at increasing temperatures.

monolith frame, there may be very little carbon between the $LiFePO_4$ and the electrolyte interface. This could potentially be improved through the addition of a carbon source in the $LiFePO_4$ precursor solution.[20−25]

Figure 6c shows the AC impedance spectroscopy results for the $LiFePO_4$/carbon composite samples. The size of the semicircle formed from the high frequency range of the data shows a good correlation with the capacity results in Figure 6a. A smaller diameter semicircle reflects lower

(18) Choi, D.; Kumta, P. N. *J. Power Sources* **2007**, *163*, 1064–1069.
(19) Mi, C. H.; Zhang, X. G.; Zhao, X. B.; Li, H. L. *J. Alloys Compd.* **2006**, *424*, 327–333.
(20) Ravet, N.; Chouinard, Y.; Magnan, J. F.; Besner, S.; Gauthier, M.; Armand, M. *J. Power Sources* **2001**, *97−8*, 503–507.
(21) Yamada, A.; Chung, S. C.; Hinokuma, K. *J. Electrochem. Soc.* **2001**, *148*, A224–A229.
(22) Chen, Z.; Dahn, J. R. *J. Electrochem. Soc.* **2002**, *149*, A1184–A1189.
(23) Dominko, R.; Bele, M.; Gaberscek, M.; Remskar, M.; Hanzel, D.; Pejovnik, S.; Jamnik, J. *J. Electrochem. Soc.* **2005**, *152*, A607–A610.
(24) Zaghib, K.; Mauger, A.; Gendron, F.; Julien, C. M. *Chem. Mater.* **2008**, *20*, 462–469.
(25) Delmas, C.; Maccario, M.; Croguennec, L.; Le Cras, F.; Weill, F. *Nat. Mater.* **2008**, *7*(8), 665–671.

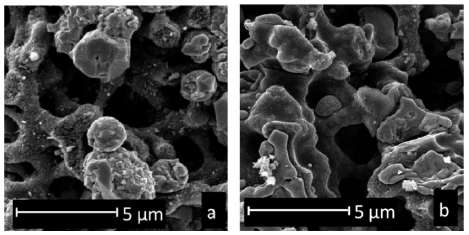

Figure 7. SEM images of $LiFePO_4$/carbon monoliths prepared with (a) F127 and (b) F108 triblock copolymer amphiphiles and calcined at 750 °C.

charge transfer impedance within the electrode material.[26] This indicates that the charge transfer resistance may be the limiting factor for the electrochemistry results. By improving the carbon coating of the $LiFePO_4$ particles, the transfer resistance between them may improve.

Amphiphile Based $LiFePO_4$/Carbon Composite Monoliths. In an attempt to improve the diffusion impedance through the $LiFePO_4$/carbon composite, triblock copolymers were added into the precursor solution so as to provide a thin carbon coating around the $LiFePO_4$ particles and improve the resistance of the system. It was also anticipated that the amphiphiles may change the surface chemistry of the precursor solution and allow improved penetration into the carbon mesopores. Either 0.02 mol of F127 or 0.01 mol of F108 per mol of $LiFePO_4$ was added to the precursor solutions and stirred for 2 h before infiltrating into the carbon monoliths. The monoliths were calcined at 750 °C under a nitrogen atmosphere.

The $LiFePO_4$/carbon monolith samples prepared with F127 and F108 block copolymers had slightly higher quantities of carbon present in the samples, 55 and 68%, respectively. The SEM images in Figure 7 show different morphology in the samples made with surfactant compared with Figure 3. The samples made with F127 feature micrometer sized $LiFePO_4$ spheres sitting among the branched carbon monolithic lattice, and smaller submicrometer crystals protrude from the carbon branches (Figure 7a). The samples prepared with F108 show more oblong shaped $LiFePO_4$. The $LiFePO_4$ particles appear to be entwined through the carbon monolith efficiently filling the macroporous space (Figure 7b).

The XRD analysis (see the Supporting Information, Figure S3) shows broad peaks around 25−35° 2θ due to the large amounts of nongraphitic carbon present. The crystallite sizes for F127 and F108 samples were 49 and 54 nm respectively, indicating that the addition of the amphiphiles in the $LiFePO_4$ precursor solution restricted crystallite growth.

The nitrogen sorption results determined that the surface areas for the F127 and F108 samples were 160 and 140 $m^2 g^{-1}$, and the pore volumes were 0.26 and 0.17 $cm^3 g^{-1}$, respectively. The desorption pore size distribution in Figure 8a shows that there is a drop in pore volume for the $LiFePO_4$/carbon composite samples compared to the carbon monolith on its own; however, there is no reduction in the pore size distribution that would be expected if the precursor solution was able to penetrate the carbon mesopores.

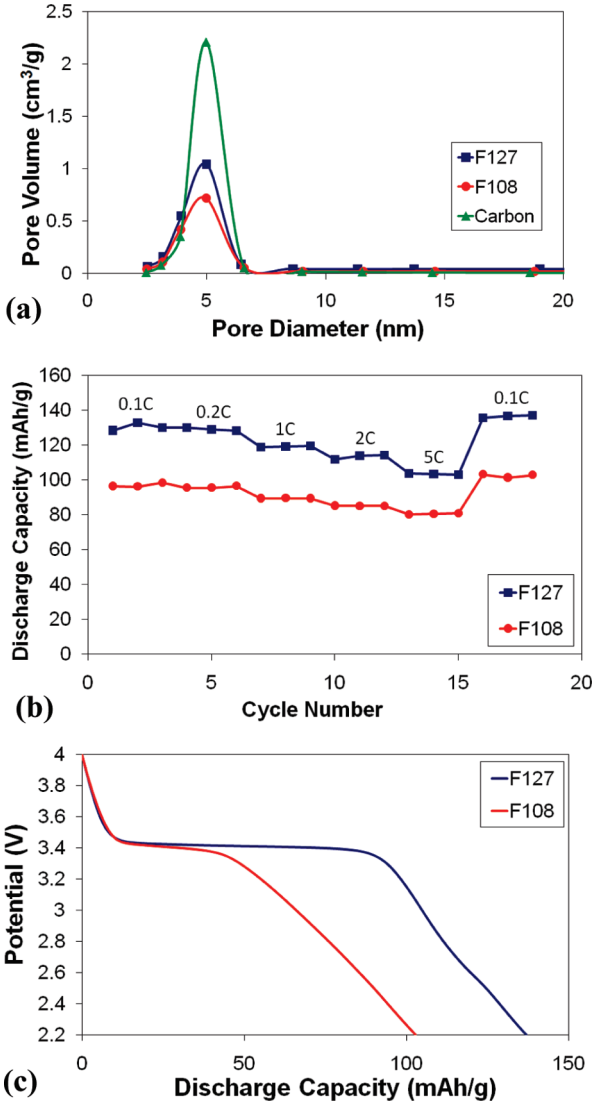

Figure 8. Characterization of the $LiFePO_4$/carbon monolith composite samples made with the addition of F127 and F108 triblock copolymer surfactants and calcined at 750 °C. (a) The BJH desorption pore size distribution along with the carbon template for comparison (the results refer to the nitrogen uptake per gram of sample ($LiFePO_4$/carbon), (b) discharge capacity, and (c) 0.1C rate discharge profiles.

The electrochemical results for the $LiFePO_4$/carbon monolith samples prepared with surfactants are shown in Figure 8b. The discharge capacities for the samples are significantly different between the two surfactants trialed. The sample made with F108 reached 100 mA h g^{-1} capacity at slow discharge rates which is 60% of the theoretical capacity. The reduced rate performance may be due to the higher levels of carbon from the surfactant compared to the F127 sample; an extra 15% carbon, left over from the F108, may lower the capacity of the cell. The sample made with F127 had similar capacities as the monolithic sample made without the surfactant signifying that the addition of surfactant to the precursor solution did not improve the capacity of the $LiFePO_4$/carbon monolith electrodes.

Analysis of the discharge profiles for the surfactant based monolith samples (Figure 8c) shows significantly

(26) Shin, H. C.; Cho, W. I.; Jang, H. *Electrochim. Acta* **2006**, *52*, 1472–1476.

improved plateaus over those seen in Figure 6b. The voltage plateau in Figure 8c was much flatter than those in Figure 6b which indicates significant reduction in the electrode polarization. The reduction in crystallite size for the samples prepared with the F127 and F108 amphiphiles (49 and 54 nm, respectively) compared to the $LiFePO_4$/carbon monolith calcined at the same temperature of 750 °C (94 nm) may account for the improved discharge profile seen in Figure 8c.

Similar discharge capacities were recently achieved by Wu et al., with their $LiFePO_4$ nanoparticles that were embedded in a nanoporous carbon matrix.[27] They reported a discharge capacity of 145 mA h g^{-1} at 0.9C as well as a sluggish discharge slope similar to that seen in Figure 8c. It is suggested that this phenomenon is comparable to that reported for other transition-metal oxide nanoparticles at low potentials[28−30] and may be caused by an energetically favored lithium-storage process. The model proposes that a charge separation occurs due to the localization of Li^+ ions on the $LiFePO_4$ particles and electrons (e^-) on the carbon matrix. As a result of the high surface areas at the interface, a supercapacitor-like phenomenon occurs.[27] When the nanoporous carbon matrix was assembled into a supercapacitor with an activated carbon counter electrode, improved energy densities were observed.[27] This phenomenon may be occurring between the $LiFePO_4$ particles and the carbon monolith which explains the slope of the discharge plateau and may be an interesting application to further investigate.

Comparisons with other high surface area nanostructured $LiFePO_4$ materials indicate that the capacity can be further improved when tested against lithium counter electrodes. In our previous work with $LiFePO_4$, we reached capacities of 160 mA h g^{-1} at 0.1C and 115 mA h g^{-1} at 5C using PMMA colloidal crystals as templates to prepare electrodes with mesopores and macropores.[14] In another investigation, a facile water based synthesis with the addition of amphiphiles was used to optimize the porous $LiFePO_4$ electrode material to obtain capacities of 165 mA h g^{-1} at 0.1C and 124 mA h g^{-1} at 5C.[15] Elsewhere, Lim et al. formed nanowire and hollow $LiFePO_4$ cathodes using mesoporous silica templates.[31] These materials featured high surface areas up to 103 m^2 g^{-1} and obtained very high capacities of 165 mA h g^{-1} at 0.5C and 153 mA h g^{-1} at 15C.[31] The materials presented in this paper did not achieve such capacities; however, the novel concept of a continuous macroporous carbon network which featured mesopores to act as a conductive monolithic current collector to which the $LiFePO_4$ infiltrated offers promising structural enhancements. Improvements may be achieved by infiltrating $LiFePO_4$ nanoparticles within the carbon monolith to improve access into the mesopores and increase the interface between the carbon and the active electrode material.

Conclusions

A novel method for preparing nanostructured materials was investigated. A carbon monolith with bimodal porosity was nanocast from a hard silica template. This carbon monolith featured a macroporous network with access to branches that contained mesopores. This type of structure is potentially ideal as an electrode material as the macroporous network allows efficient percolation of the electrolyte through the electrode improving the electrolyte access to the mesopores while providing a conductive framework with intimate contact with the $LiFePO_4$. A composite $LiFePO_4$/carbon material was prepared as a means to employ the conductive carbon monolith as the current collector to which the lithium iron phosphate can infiltrate. This enables the high surface areas to be maintained while keeping a nanostructured monolith for use as a cathode material for lithium ion batteries.

Electrochemical results for the composite monolith electrodes reported here showed discharge capacities for $LiFePO_4$ of 140 mA h g^{-1} at 0.1C and 100 mA h g^{-1} at fast discharge rates of 5C. In the future, improvements to the electrochemistry may be achieved by obtaining a more consistent coating of lithium iron phosphate surrounding the carbon monolith mesopores. This would increase the carbon−$LiFePO_4$ interface and potentially improve the charge transfer kinetics. Further investigation into the application as a supercapacitor electrode material may also be promising.

Acknowledgment. C.J.D. is the recipient of an Australian Research Council Federation Fellowship. C.M.D. is the recipient of a CSIRO PhD scholarship and received further financial support in terms of a University of Melbourne/CSIRO Collaborative Research Grant Scheme, an Albert Shimmins Writing-up Award, a Postgraduate Overseas Research Experience Scholarship from The University of Melbourne for travel to The Max Planck Institute of Colloids and Interfaces, and an Australian Institute of Nuclear Science and Engineering award (AINGRA07027) for access to research equipment at the Australian Nuclear Science and Technology Organisation. We thank Mr. Mark Blackford for the TEM measurements and Dr. Anthony Hollenkamp, Dr. Gregory Wilson, and Arek Liewendewski for assistance with optimization of the electrode and coin cell fabrication.

Supporting Information Available: The BJH pore size distribution of the silica and carbon monoliths taken from the desorption branch of the isotherm; nitrogen sorption isotherms for $LiFePO_4$/carbon monolith composites calcined at increasing temperatures; and XRD analysis and AC impedance spectroscopy for the $LiFePO_4$/carbon monolith composite samples made with triblock copolymer surfactants (PDF). This material is available free of charge via the Internet at http://pubs.acs.org.

(27) Wu, X. L.; Jiang, L. Y.; Cao, F. F.; Guo, Y. G.; Wan, L. J. *Adv. Mater.* **2009**, *21*, 2710–2714.
(28) Balaya, P.; Li, H.; Kienle, L.; Maier, J. *Adv. Funct. Mater.* **2003**, *13*, 621–625.
(29) Jamnik, J.; Maier, J. *Phys. Chem. Chem. Phys.* **2003**, *5*, 5215–5220.
(30) Maier, J. *Nat. Mater.* **2005**, *4*, 805–815.
(31) Lim, S. Y.; Yoon, C. S.; Cho, J. P. *Chem. Mater.* **2008**, *20*, 4560–4564.